nature energy

Analysis

https://doi.org/10.1038/s41560-024-01701-9

Critically assessing sodium-ion technology roadmaps and scenarios for techno-economic competitiveness against lithium-ion batteries

Received: 12 June 2024

Accepted: 13 December 2024

Published online: 13 January 2025

Check for updates

Adrian Yao [1,2] ✉, Sally M. Benson[3] & William C. Chueh [1,2,3] ✉

Sodium-ion batteries have garnered notable attention as a potentially low-cost alternative to lithium-ion batteries, which have experienced supply shortages and price volatility for key minerals. Here we assess their techno-economic competitiveness against incumbent lithium-ion batteries using a modelling framework incorporating componential learning curves constrained by minerals prices and engineering design floors. We compare projected sodium-ion and lithium-ion price trends across over 6,000 scenarios while varying Na-ion technology development roadmaps, supply chain scenarios, market penetration and learning rates. Assuming that substantial progress can be made along technology roadmaps via targeted research and development, we identify several sodium-ion pathways that might reach cost-competitiveness with low-cost lithium-ion variants in the 2030s. In addition, we show that timelines are highly sensitive to movements in critical minerals supply chains—namely that of lithium, graphite and nickel. Our modelled outcomes suggest that being price advantageous against low-cost lithium-ion variants in the near term is challenging and increasing sodium-ion energy densities to decrease materials intensity is among the most impactful ways to improve competitiveness.

The energy transition requires massive deployment of batteries for electric vehicles (EVs) and stationary energy storage systems (ESS). Lithium-ion (Li-ion) batteries have been responsible for nearly all new deployments of storage in recent years[1–3], largely enabled by the tremendous cost declines over the past three decades of commercialization characterized by an aggressive learning rate where prices have fallen by more than 97% since they were first commercialized in 1991[4,5]. This trend is reflected in the average Li-ion cell prices shown in Supplementary Fig. 1 aggregated from the industry data contributors to this work[1–3,6], which also resolves the diverging price trajectories of NMC-type (nickel manganese cobalt oxide) and LFP-type (lithium iron phosphate) cathode chemistries. However, rapid Li-ion demand growth has recently placed a substantial burden on the minerals supply chain—namely that of lithium, nickel, graphite and cobalt—resulting in a first-ever increase in the average Li-ion cell price index in 2022[3], which subsequently fell again as minerals prices plummeted[7–9]. This has prompted some to escalate concerns regarding the possible overdependence on Li-ion and risks of production bottlenecks, supply chain shocks and geopolitical constraints.

Sodium-ion (Na-ion) batteries present a potentially viable near-term substitute for Li-ion for two primary reasons: (1) increased

[1]Department of Materials Science and Engineering, Stanford University, Stanford, CA, USA. [2]Applied Energy Division, SLAC National Accelerator Laboratory, Menlo Park, CA, USA. [3]Department of Energy Science and Engineering, Stanford University, Stanford, CA, USA. ✉e-mail: ayao2@stanford.edu; wchueh@stanford.edu

abundance and availability of sodium suggests lower prices and (2) drop-in compatibility with Li-ion manufacturing infrastructure suggests rapid scaling timelines. Therefore, in response to severe post-COVID lithium price spikes, manufacturers recently announced over 240 GWh of Na-ion cell manufacturing pipeline through 2030[10], promising lower prices than Li-ion. However, exactly if, when and by how much Na-ion batteries will be price advantageous is still largely a matter of speculation.

Learning curves have been widely used in forecasting technological progress and price since patterns of improvement were first postulated by Wright for manufacturing airplanes[11]. The typical learning curve (Wright's law) predicts price reductions as a function of cumulative production ('learning-by-doing') and has been statistically shown to produce accurate forecasts across wide-ranging sectors[12], including energy technologies[13]. Given the industrial importance of Li-ion batteries, several studies have sought to characterize their price trends using the conventional form of Wright's law[4,14–16] (equation (1) in Methods), whereas others have ascribed additional descriptors, such as learning-by-researching or economies-of-scale, to understand their historic trends[4,5,17]. However, conventional learning curves unrealistically assume infinite cost reductions approaching zero, which neglects limits set by underlying minerals. Therefore, yet other approaches have sought to additionally constrain the learning curve with a minerals price floor to produce more realistic projections[18,19]. It is worth noting that not all price floors or additional parameters can be assumed to be effective. Price floors based on expert opinion, for example, have historically been shown to be unrealistic[20], and extra parameters have been shown to reduce model performance owing to overfitting[12].

In this work, we propose an approach that combines componential, floor-constrained learning curves for individual material components with technical development roadmaps that also exhibit learning behaviour to better forecast future price trends—balancing model simplicity and physical accuracy. We then use this approach to forecast battery price trends for Li-ion and Na-ion under various technological, market and supply chain conditions to identify strategies that improve the techno-economic competitiveness of Na-ion.

Combining learning curves with technology roadmaps

We construct historical and forecasted aggregate price curves by incorporating knowledge of both (a) material component prices (in $\$\ kg^{-1}$ or $\$\ m^{-2}$), which evolve via learning-by-doing as a function of cumulative experience, and (b) materials intensities (kg kWh^{-1}), which evolve due to continued cell engineering and materials advancements as a function of time. We institute practical floors for both—using minerals price floors for the former and engineering limits for the latter. This approach thus combines a modified Wright's law and a modified Moore's law, represented by equations (3) and (4) in Methods, respectively.

For each material component in a battery cell, we construct individual learning curves and institute a price floor based on their known elemental composition of benchmarkable key minerals, which dynamically evolve with time. Therefore, each of our material component costs comprises two elements: (1) a fluctuating materials price floor representing the weighted sum of underlying minerals from a time series of historical and forecasted prices, and (2) decreasing costs of non-mineral inputs represented by a learning curve that scales with historical and forecasted market share. Non-mineral inputs include costs associated with capital equipment, operating costs, production scrap from yield, chemical conversion inefficiencies and others. The downward trajectory of the learning curve component is consistent with expectations of technological improvements owing to processing innovation and optimization as well as implicit assumptions of economies-of-scale. By contrast, market-driven volatility is expected in the materials price floor component. This approach is analogous to previous literature decomposing coal-fired electricity generation costs into a 'noisy' price floor of fuel commodities and improving costs of plant construction owing to technological learning[19]. In this case, however, we do not disaggregate the materials component learning curves further into the technical factors identified above, and we highlight this area for future work.

Once the floor-constrained learning curves are obtained for each material component, they are subsequently summed according to their mass or areal intensities derived from physically accurate cell modelling. To capture the steady decreases in materials intensities over time (which have contributed greatly to Li-ion price declines so far[4,5]), we model cell designs in a bottoms-up fashion that are representative of past commercial products, present state-of-the-art and future designs considering anticipated improvements for materials performance and cell engineering. On the basis of differences in materials intensities between cell designs, which are each ascribed to a point in time, we construct roadmaps by fitting curves with asymptotic limits defined by theoretical or practical engineering limits. This approach is similar to previous literature disaggregating solar photovoltaic device-level price reductions based on observable technical factors such as silicon consumption and wafer sizes[21]. However, in this work, we add resolution by fitting materials intensity curves for each component based on bottoms-up modelling, and we do not decompose the costs of manufacturing further into other technical factors. We justify this based on knowing that battery cell costs are dominated by their bill-of-materials, and we seek to specifically probe how materials and cell design improvements can alter price trajectories. Our modelled manufacturing overhead cost trends therefore include cost savings from improved processing yield and economies-of-scale. To obtain bill-of-materials and manufacturing costs, we leverage the Battery Performance and Cost (BatPaC) process-based model[22] developed by Argonne National Laboratory to recreate cell designs (Methods). As BatPaC specifically models state-of-the-art manufacturing, we only use the manufacturing overhead cost component of present-day cell designs and subsequently fit learning curves against historical data on manufacturing costs to estimate future trends.

Our models rely upon a wide-ranging collection of sources obtained from industry data contributors to ensure accuracy and relevance. They include Benchmark Mineral Intelligence, Wood Mackenzie, BloombergNEF, Avicenne Energy, S&P Global and other commercial reports[23,24] (Supplementary Table 1 summarizes the data sources of key mineral inputs). In addition, we validate and confirm accuracy and relevance by surveying a panel of industry experts to obtain inputs on realistic price figures, state-of-the-art cell designs and production costs[25].

Establishing Li-ion baselines

We divide the effort to construct Li-ion baseline curves into two parts as discussed above: (a) establishing floor-constrained materials component learning curves and (b) establishing physically accurate technology roadmaps. We define 2023 as present day. Previous years are designated historical and static, which inform parameter fitting. Forward years are projected, driven by the inputs of minerals pricing and market growth forecasts.

Li-ion materials component learning curves

An example procedure for establishing the floor-constrained materials component learning curves is illustrated in Fig. 1 for NMC cathode material. Historical price assessments were tabulated from industry and literature sources to establish a time series starting at or before 2010[2,5,23,26,27]. We also collected data on historical production quantities to enable calculation of cumulative 'experience'. Both are shown in Fig. 1a. Historical pricing for key minerals were obtained from industry data contributors[1,2,28,29]. Historical prices were also collected from the United States Geological Survey (USGS) mineral commodity summaries dating back to 1991[30], and all price figures were inflation-adjusted

https://doi.org/10.1038/s41560-024-01701-9

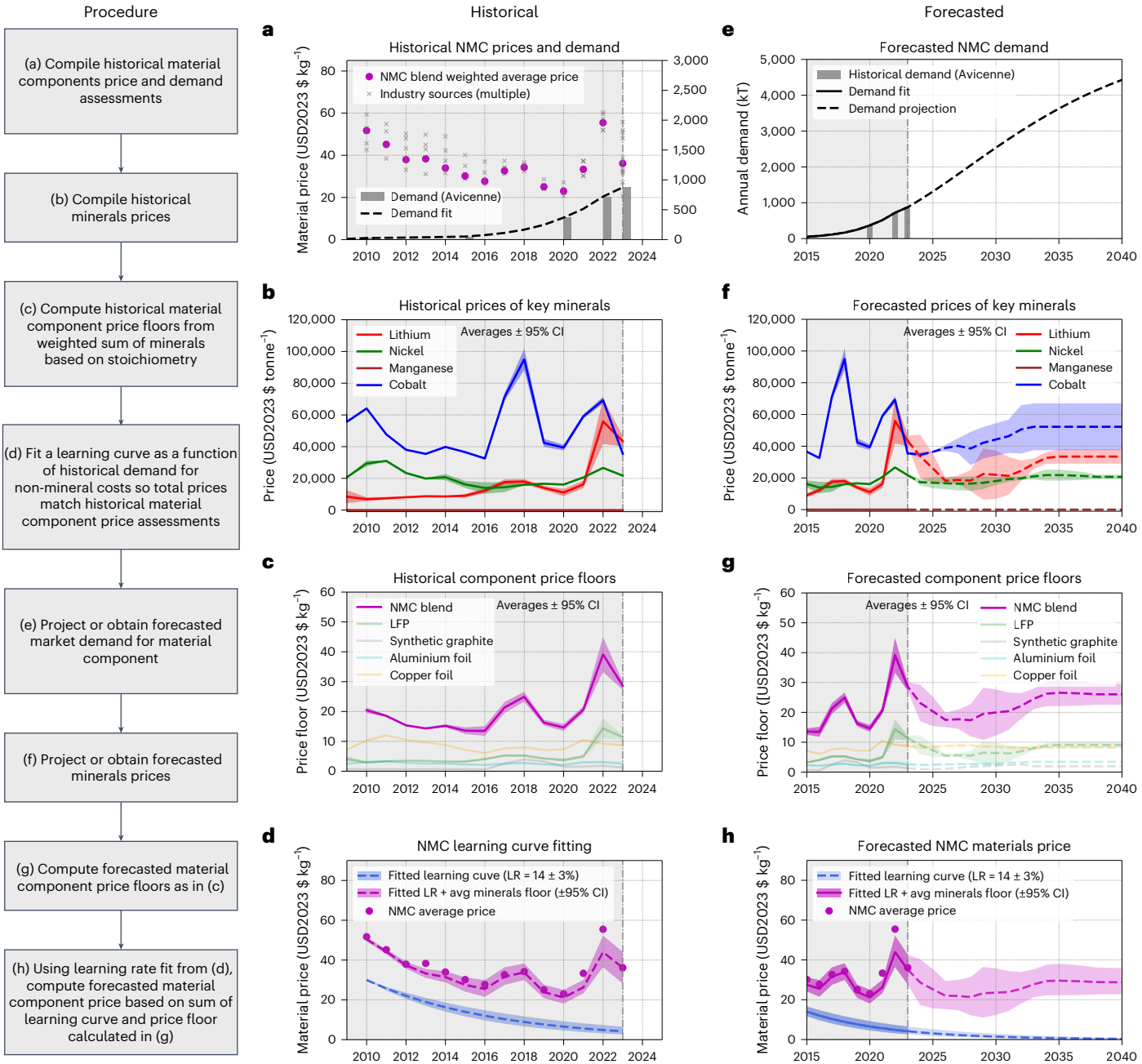

Fig. 1 | Establishing floor-constrained materials component learning curves. A step-by-step process (flowchart in the left column) of fitting material component learning rates based on historical data (centre column) and then projecting future materials prices based on forecasted demand and minerals prices (right column). **a**, Historical material component price assessments for NMC cathode active material mapped against historical material demand obtained from industry sources. **b**, Historical prices of key benchmarkable minerals in NMC—namely lithium, nickel, manganese and cobalt—obtained from industry sources. Shaded regions show 95% CI. **c**, Historical material component price floors representing a weighted sum of underlying minerals according to their stoichiometric ratios. See Supplementary Note 2 and Supplementary Figs. 4 and 5 for details on capturing the evolution in NMC stoichiometry—represented here as an 'NMC blend'. Price floors of other material components also shown. **d**, Fitting a learning curve for the non-mineral cost components of NMC. Combining the learning curve with the price floor shown in **c**, a total material component price can be obtained, which agrees with historical price assessments. **e**, Forecasted demand for NMC material based on market projections obtained from industry partners. **f**, Forecasted minerals prices for the same key elements in **b** obtained from industry partners. **g**, Calculated material component price floors based on forecasted minerals prices. **h**, Forecasted material component prices obtained by combining the price floor shown in **g** with a continuation of the same learning curve obtained in **d** while keeping the learning rate parameter fixed. We recognize here our assumptions that learning rates remain fixed over a forecasted timespan longer than the fitted historical data. Long-term minerals price forecasts are also based on expert opinion of industry partners. Therefore, these forecasted prices represent a simulated future based on best knowledge today. See Supplementary Note 4 for additional high/mid/low minerals price simulations.

to USD2023. Aggregated minerals prices are shown in Supplementary Fig. 2, but a subset of the benchmarkable minerals comprising NMC—lithium, nickel, manganese and cobalt—are shown in Fig. 1b. Subsequently, the weighted sum of each mineral component is added according to their stoichiometric ratios to produce a material component price floor, shown in Fig. 1c (see Supplementary Note 1 for additional details, Supplementary Table 2 for a comprehensive list of material components and their compositions, and Supplementary Fig. 3

for calculated component price floors for key materials). For NMC-type materials that have historically experienced an evolution in stoichiometry, we take a volume-weighted average of each 'nodal' composition to reflect a representative blend at every time step (Supplementary Note 2 and Supplementary Figs. 4 and 5). Finally, with knowledge of component price floors, actual historical price assessments and cumulative production experience, this sufficiently constrains the modified Wright's law to leave the learning rate as the only fitting parameter, per equation (3) in Methods. The learning curve then represents the non-mineral costs associated with the material component and is fit in a way so that the total (price floor + learning curve) matches historical price assessments, shown in Fig. 1d. See Supplementary Note 3 for additional comments on sources of uncertainty given data scarcity.

Once a characteristic learning rate is established, forecasting future prices can be performed based on forecasted market growth and minerals pricing, assuming that learning rates do not change. It is worth noting that endogeneity is expected between the two, but we leave them independent. In addition, we recognize that the forecasted timespan is longer than that of the historical data used to fit the constant learning rate, but this provides a first-order approximation sufficient for future simulation purposes. Forecasted Li-ion market growth from several market intelligence sources were approximated with Gompertz functions to obtain continuous curves (Methods and Supplementary Fig. 6), where the 'LIB Base Case' scenario assumes no appreciable Na-ion deployment and LFP market penetration reaching 50% market share saturation by 2050 (Supplementary Fig. 7). This can then be translated to NMC demand in Fig. 1e by mass. Forecasted minerals prices are again provided by data contributors and aggregated in Fig. 1f. As predicting future price movements of key minerals is inherently challenging, we also separately model fixed-price high/mid/low forecasted scenarios for lithium and nickel to test sensitivity (Supplementary Note 4 and Supplementary Figs. 8 and 9). Material component price floors can again be calculated (Fig. 1g). To ensure continuity between historical and forecasted materials price time series, both were constrained to converge on present-day (2023) pricing, which were obtained from various industry sources and aggregated for robustness[2,23,25–27] (a summary of Li-ion component price assessments is presented in Supplementary Fig. 10). The final result is a material component price forecast that is responsive to dynamic minerals price movements as well as market penetration (Fig. 1h).

We repeat the above procedure for a full set of material components used in Li-ion batteries, including various cathode material chemistries. Whereas NMC was used as an illustrative example above, hereafter we focus on LFP in the Main Text as it is widely considered the more relevant comparison with Na-ion with respect to performance and cost. Using the same methodology, the price forecast for LFP material is shown in Fig. 2a. The remaining material price curves are presented in Supplementary Figs. 11–18, and their fitted learning rates are summarized in Fig. 2b compared with average historical Li-ion learning rates aggregated from previous literature[3,4,14,15,17].

Li-ion technology roadmaps

To establish Li-ion technology roadmaps, physically accurate models of NMC and LFP cell designs representing past and present were developed. Present cell designs were modelled based on recent teardowns of state-of-the-art commercial cells published in literature[31–33]. Past cell designs were also modelled based on previously published commercial cell teardowns in literature and industry reports documenting engineering progress at the time of their publication[34–36] (Supplementary Figs. 19–23). This enabled fitting of materials intensity trends that correspond with development roadmaps (Supplementary Figs. 24 and 25). Note here that we do not model next-generation Li-ion roadmaps (lithium manganese iron phosphate cathodes, silicon anodes and so on), which could substantially reduce materials intensity. Thus, our analysis presents a conservative case of anticipated price reductions for Li-ion.

Finally, combining material component price forecasts and materials intensity roadmaps per equation (12), complete Li-ion price curves were constructed as shown in Fig. 2c for LFP (NMC component curve stack-up shown in Supplementary Fig. 26). The final LFP price curve is shown in Fig. 2d with predicted prices reaching \$51 kWh^{-1} by 2030 assuming that lithium prices at the time are just under \$22,000 $tonne^{-1}$ (and as low as \$45 kWh^{-1} if lithium prices are ~\$10,500 $tonne^{-1}$ per the low price scenario in Supplementary Fig. 8 and Supplementary Note 4). Supplementary Fig. 27 shows LFP and NMC price forecasts combined.

Deconvoluting the sources of learning

Examining the fitted componential learning rates, learning rates appear correlated with processing complexity, which may be anecdotally associated with the number of required control parameters during production (a clearer definition and correlation of complexity to learning rate is a subject of future work). Higher complexity processes (for example, cathode synthesis and cell assembly) tend to have higher rates of learning, whereas lower complexity processes (for example, metal foil and anode production) tend to have lower rates (see Supplementary Note 5 for further discussion). However, compared with previous literature on Li-ion learning rates, we observe that our componential learning rates are all lower than the aggregate average rate experienced by historical cell prices (Fig. 2b) of 21.1 ± 3.7% (refs. 3,4,14,15,17), which suggests that there must be another key contributor responsible for the aggressive price reductions in Li-ion. This can be explained by the technical advancements in the design of Li-ion cells over the past several decades, now requiring substantially lower materials intensity on a per-kWh basis than before[4,5]. Specifically, the shift from cells optimized for power to those optimized for energy enabled higher active material utilization[5,16,36]. The steady improvements to material specific capacities have also contributed to this phenomenon.

Therefore, the aggressive Li-ion price trends appear to be a story of modest price reductions in materials from learning-by-doing compounded by substantial engineering advancements and learnings. This deconvolution of the traditional learning model into key constituent contributors is an important nuance to forecast realistic price trends of incumbent and emerging technologies such as Li-ion and Na-ion, respectively. To illustrate, Fig. 2d additionally compares price forecasts of LFP cells using our method—accounting for minerals price and engineering design floors—against the typical unconstrained single-factor learning curve form of Wright's law (equation (1) in Methods) utilizing the historical average Li-ion rate. This curve nearly intersects the calculated LFP minerals price floor in 2050, which may be unrealistic and overly optimistic.

Forecasting Na-ion cell development roadmaps

Like Li-ion, Na-ion is an umbrella term encompassing several material chemistries generally categorized by cathode material classes. They include transition metal layered oxides, polyanions and Prussian Blue analogues[37]. Recent commercialization efforts indicate strong momentum behind (i) layered oxides with a general formula of $Na_x(M)O_2$ ($x \sim 1$, M = Ni, Fe, Mn, Cu) with $NaNi_xMn_y(M)_{1-x-y}O_2$ (NaNM) being the most common and (ii) vanadium-free mixed polyanions with the formula $Na_4Fe_3(PO_4)_2(P_2O_7)$ (NFPP)[25]. In almost all instances, disordered hard carbons (HCs) are used as Na-ion anode materials instead of the crystalline graphite used in Li-ion batteries owing to their low sodium storage capacities[38]. Alternative anodes to HCs include emerging technology directions such as (i) metallic tin (Sn) that alloys with sodium[39] or (ii) 'anode-free' configurations that electrodeposit and strip sodium metal directly on current collectors[40,41]. Here, in reference to NaNM, we specifically model $NaNi_{0.33}Mn_x(M)_{0.67-x}O_2$, where M includes Mg and Ti dopants and that are currently being commercialized[42–44]. As the non-nickel transition metals contribute negligible minerals costs and redox activity[44], our NaNM archetype also functionally represents compositions such as $NaNi_{0.33}Fe_{0.33}Mn_{0.33}O_2$ (NFM111). Given the recent

https://doi.org/10.1038/s41560-024-01701-9

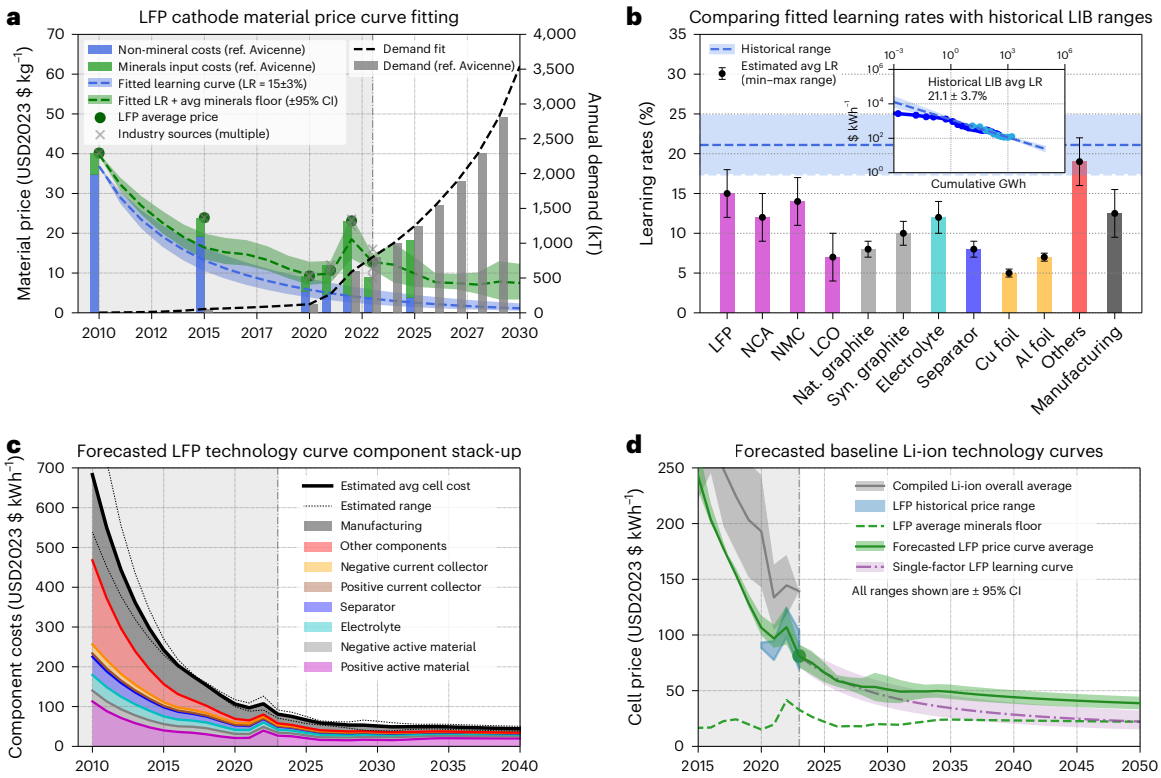

Fig. 2 | Componential floor-constrained construction of technology price curves. a, Example material component price curve generation for LFP material. A learning curve (in blue) is fit against historical conversion cost data to capture experience as cumulative production increases (grey bars and dashed black line), while a minerals price floor (in green) rides upon the learning curve. Reasonable agreement between the generated price curve and average prices collected from industry sources is observed. **b**, Fitted learning rates for key Li-ion battery (LIB) material components (NCA, nickel-cobalt-aluminium oxide; LCO, lithium cobalt oxide; Nat. graphite, natural graphite; Syn. graphite, synthetic graphite) compared against the historical average learning rate (LR) for Li-ion compiled from literature and industry reports—shown in inset. See Supplementary Note 5 for details. **c**, Total price curve for LFP-type cells constructed by summing up all constituent material components based on cell design models that inform materials intensity per energy content stored. See Supplementary Fig. 26 for equivalent plots for NMC. **d**, Forecasted LFP Li-ion price curve for the baseline scenario, showing good agreement with historical averages. A typical single-factor learning curve using the historical average learning rate (established in **b**) is also shown for comparison with potentially overly optimistic outcomes. CIs capture underlying uncertainty in minerals prices, starting materials prices and learning rates.

interest in replacing nickel with earth-abundant elements such as iron and manganese owing to high costs, we also model a material such as $Na_{0.67}Fe_{0.5}Mn_{0.5}O_2$ (NaFM). However, as these materials still suffer from unresolved performance challenges, we model technical roadmaps that gradually reduce nickel to 0% by ~2040 (Supplementary Note 6 and Supplementary Figs. 28 and 29)—analogous to the gradual reduction of cobalt content in NMC cathodes over the years. This is modelled separately from roadmaps that maintain a static 33% nickel stoichiometry.

The three key market segments modelled were stationary ESS, two/three-wheelers and micromobility (TTW/MM), and EVs. Specifically, we consider three hypothetical Na-ion market growth scenarios with increasing degrees of penetration, ranging from the most conservative, 100% Na-ion penetration into ESS by 2040, to the most aggressive, 100% penetration into ESS by 2035, 100% of TTW/MM by 2040 and 25% EVs by 2040 (Supplementary Fig. 6). Note that the most conservative market penetration scenario matches more closely to forecasts provided by industry data contributors.

Given the importance of capturing engineering advancements on techno-economics, we model a multitude of Na-ion cell development roadmaps for NaNM|HC, NaFM|HC, NFPP|HC, NaNM|Sn, NaFM|Sn, NFPP|Sn, NaNM|Anode-free and NaFM|Anode-free cell designs (see Supplementary Figs. 30–47 for details on 18 different Na-ion cell designs and Supplementary Figs. 48–60 for details on modelled roadmaps). These roadmaps assume gradual improvements from state-of-the-art 2024 designs towards future technical advancements by 2030 that increase energy densities and thereby reduce prices. See Methods for details on fitting trends with a modified Moore's law. A summary of the modelled technical roadmaps is tabulated in Table 1.

Evaluating Roadmap 'NaNM|HC 7' as an example: a NaNM|HC Baseline cell design (Supplementary Fig. 30) evolves to experience an increase in HC specific capacity from 330 mAh g^{-1} to 400 mAh g^{-1}, an increase in cell operating voltage from 4.0 V to 4.2 V, and a 20% increase to NaNM specific capacity (to ~175 mAh g^{-1} measured from 2.0 V to 4.25 V) (Supplementary Fig. 36)—all by 2030. The resulting materials intensity trends are shown in Fig. 3a. Pricing for key Na-ion materials components are obtained by surveying industry expert sources to ensure commercial relevance[25] (Methods). These values are summarized in Fig. 3b. Applying various learning rates and market growth assumptions, we forecast Na-ion price curves via our componential construction methodology. Figure 3c illustrates a scenario with the most conservative market penetration (100% Na-ion penetration into ESS by 2040; Supplementary Fig. 6) and with novel cumulative experience applied to the anode material only (Supplementary Note 7).

It is worth highlighting our key assumptions. Here we assume (1) drop-in compatibility with existing Li-ion manufacturing infrastructure, which implies immediate high-yield production and no new manufacturing learnings (Supplementary Note 7 and Supplementary Fig. 61), (2) decoupled market penetration and technology pricing, whereby endogeneity captured within a typical demand curve is ignored for the sake of modelling and understanding intervention opportunities, and (3) transferable learning rates from Li-ion to Na-ion, where cathodes, anodes and other components learn at their same

https://doi.org/10.1038/s41560-024-01701-9

Table 1 | Summary of modelled Na-ion technical development roadmaps including gravimetric and volumetric energy densities (GED and VED) of modelled large-format pouch cells

Roadmap name	Starting cell design (2024)		Improved cell design (2030)	GED/VED Wh kg^{-1})/(Wh l^{-1})	
				2024	2030
NaNM|HC 0	NaNM|HC Baseline	⇒	NaNM|HC Baseline (no improvements)	134/272	
NaNM|HC 1	NaNM|HC Baseline	⇒	Increased electrode loadings	134/272	142/295
NaNM|HC 2	NaNM|HC Baseline	⇒	Anode capacity increase to 400 mAh g^{-1}	134/272	157/325
NaNM|HC 3	NaNM|HC Baseline	⇒	Cathode 20% capacity increase	134/272	160/314
NaNM|HC 4	NaNM|HC Baseline	⇒	Anode and cathode capacity increase	134/272	174/347
NaNM|HC 5	NaNM|HC 4.2 V Baseline	⇒	Anode and cathode capacity increase at 4.2 V	134/272	196/376
NaNM|HC 6	NaNM|HC Baseline	⇒	Anode capacity increase to 400 mAh g^{-1} at 4.2 V	134/272	181/359
NaNM|HC 7	NaNM|HC Baseline	⇒	Anode and cathode capacity increase at 4.2 V	155/303	196/376
NaFM|HC 1	NaFM|HC Baseline	⇒	Increased electrode loadings	134/272	142/295
NaFM|HC 2	NaFM|HC Baseline	⇒	Anode capacity increase to 400 mAh g^{-1}	134/272	157/325
NaFM|HC 3	NaFM|HC Baseline	⇒	Cathode 20% capacity increase	134/272	160/314
NaFM|HC 4	NaFM|HC Baseline	⇒	Anode and cathode capacity increase	134/272	174/347
NaFM|HC 5	NaFM|HC 4.2 V Baseline	⇒	Anode and cathode capacity increase at 4.2 V	134/272	196/376
NaFM|HC 6	NaFM|HC Baseline	⇒	Anode capacity increase to 400 mAh g^{-1} at 4.2 V	134/272	181/359
NaNM|Sn 0	NaNM|Sn Baseline	⇒	NaNM|Sn Baseline (no improvements)	185/476	
NaNM|Sn 1	NaNM|Sn Baseline	⇒	Cathode 20% capacity increase	185/476	216/551
NaFM|Sn 0	NaFM|Sn Baseline	⇒	NaFM|Sn Baseline (no improvements)	185/476	
NaFM|Sn 1	NaFM|Sn Baseline	⇒	Cathode 20% capacity increase	185/476	216/551
NFPP|HC 0	NFPP|HC Baseline	⇒	NFPP|HC Baseline (no improvements)	111/210	
NFPP|HC 1	NFPP|HC Baseline	⇒	Increased electrode loadings	111/210	119/226
NFPP|HC 2	NFPP|HC Baseline	⇒	Anode capacity increase to 400 mAh g^{-1}	111/210	126/241
NFPP|Sn 0	NFPP|Sn Baseline	⇒	NFPP|Sn Baseline (no improvements)	137/305	
NFPP|Sn 1	NFPP|Sn Baseline	⇒	Increased electrode loadings	137/305	147/330
NaNM|AF 0	NaNM|Anode-free Baseline	⇒	NaNM|Anode-free Baseline (no improvements)	207/547	
NaNM|AF 1	NaNM|Anode-free Baseline	⇒	Increased electrode loadings	207/547	239/635
NaNM|AF 2	NaNM|Anode-free Baseline	⇒	Cathode 20% capacity increase	207/547	283/734
NaFM|AF 0	NaFM|Anode-free Baseline	⇒	NaFM|Anode-free Baseline (no improvements)	207/547	
NaFM|AF 1	NaFM|Anode-free Baseline	⇒	Cathode 20% capacity increase	207/547	283/734

respective rates between the two alkali chemistries. This last assumption may be supported by the earlier observation that materials production with similar degrees of process complexity have similar rates of learning (Supplementary Note 5), but more aggressive learning rates are also evaluated in our scenarios analysis below. We note that the first two assumptions enable a best-case scenario to model Na-ion's techno-economic competitiveness as a starting point. In addition, we do not include next-generation Li-ion roadmaps (lithium manganese iron phosphate cathodes, silicon anodes and so on) to again evaluate a best-case scenario for Na-ion. We finally emphasize that here we are only assessing the technologies at the cell level with the price of stored energy ($ kWh^{-1}) as the primary figure of merit. Therefore, this work does not capture systems-level considerations (for example, potential savings on pack integration owing to enhanced safety or reduced thermal management) or alternative performance-enabled economic considerations (for example, potentially lower levelized price of storage owing to increased cycle life). We address these additional complexities in future work.

Modelling scenarios to find conditions for competitiveness

Using the above approach, we evaluate 6,048 combinations of scenarios, all assuming GWh-scale production for Na-ion commences in 2024. The scenario variables evaluated are detailed in Supplementary Table 3. For each scenario, the Li-ion and Na-ion price curves are calculated and compared, producing plots exemplified by those shown in Fig. 4a. This example illustrates a 'NaFM|HC 2' roadmap where an initially 33% nickel stoichiometry cathode evolves to ~0% by 2040 while maintaining the same specific capacity, and an HC anode evolves to increase its specific capacity to 400 mAh g^{-1} by 2030. Owing to the reduction in nickel content, the minerals price floor decreases substantially between 2024 and 2035.

Given that the forecasted curves carry uncertainty from confidence intervals (CIs) of minerals prices (Supplementary Fig. 2), starting materials prices (Fig. 3b) and learning rates (Fig. 2b), we use methods established in previous forecasting literature[45] to quantify expected timelines for price parity and advantage by calculating the probability at each time step that one technology is lower priced than the other. These probability plots are shown in the right-hand side of Fig. 4a,b comparing LFP against the modelled example Na-ion scenarios. We further define a 'Price Parity' condition as the point in which Na-ion has ≥20% probability of being lower priced than LFP, and a 'Price Advantage' condition when that probability exceeds 80%. The yellow hatched regions in Fig. 4a,b therefore mark the periods in which a Na-ion technology and LFP are competitive in pricing and may be considered substitutes, performance notwithstanding.

https://doi.org/10.1038/s41560-024-01701-9

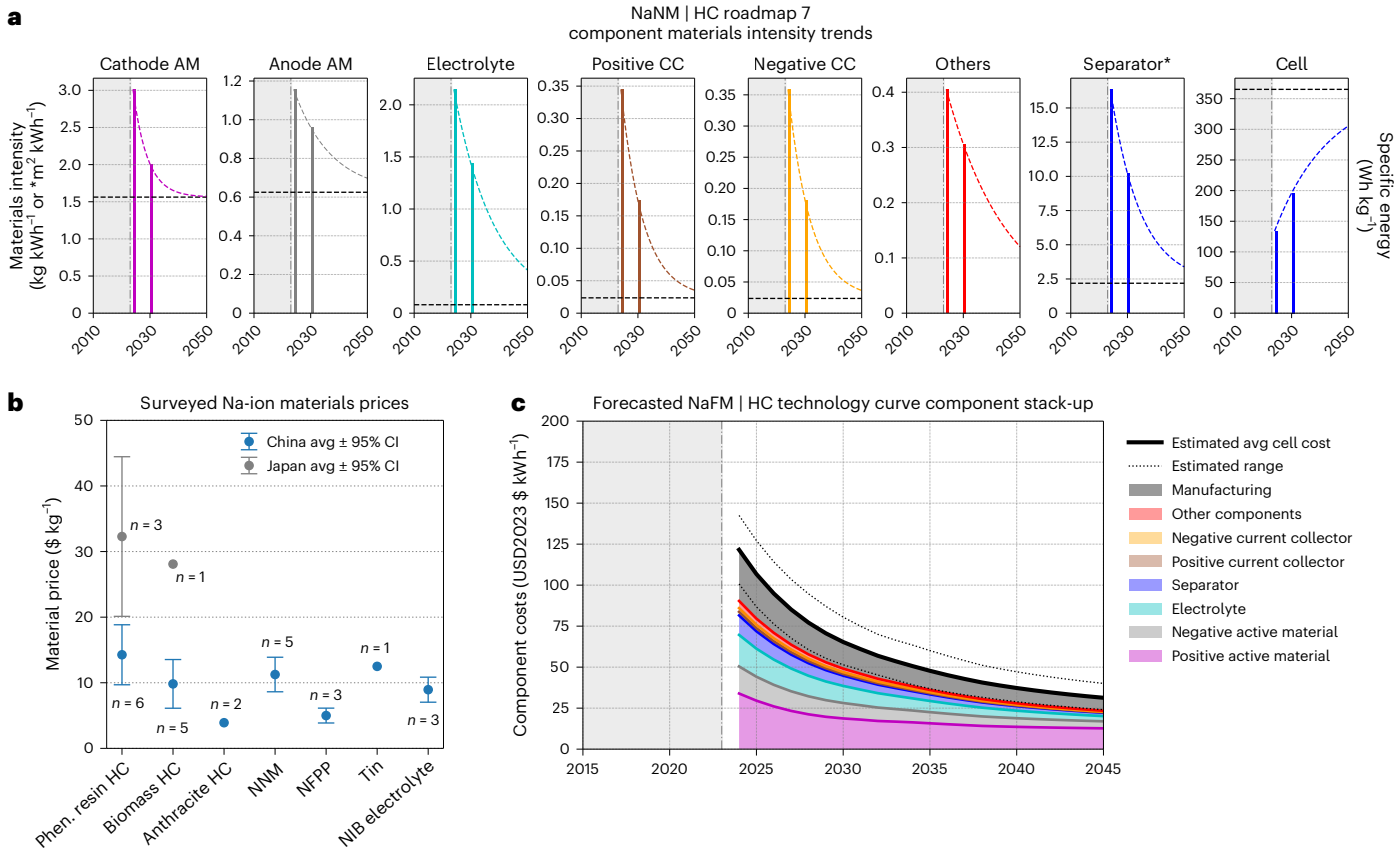

Fig. 3 | Exemplary Na-ion price curve construction based on cell modelling, road mapping and realistic materials price assessments. a, Fitted materials intensity trends that approach asymptotic engineering floors (horizontal dashed lines), shown here for Roadmap 'NaNM|HC 7'. AM, active material; CC, current collector. **b**, Surveyed price assessments for present-day Na-ion materials. The number of surveyed sources per material component (*n*) are also shown, and the 95% CI indicates the high- and low-range estimates of prices. Note that each source may provide more than one value if also providing a range (Methods). Phen., phenolic. **c**, Componential construction of Na-ion price curve for given technical roadmap. Predicted bounds illustrate CIs on the total curve from underlying uncertainty in minerals prices, starting materials prices and learning rates.

Figure 4b models an identical set of assumptions as Fig. 4a with the exception of a hypothetical graphite supply shock in 2027 that causes a permanent offset in prices but continues to learn at the same rate (see Supplementary Note 8 and Supplementary Fig. 62 for details). This enables analysis of techno-economic competitiveness and risk considering potential supply chain disruptions. In the absence of a graphite supply shock condition as illustrated in Fig. 4a, the Price Parity timeline is extended from 2032 to 2035, and the Price Advantage timeline is delayed substantially from 2038 to 2047. This large disparity is a result of the similar slopes of the price curves, which are nearly coinciding during this period.

Discussion

It is worth emphasizing that whereas our approach enables calculation of timelines to Price Advantage, the primary value proposition is understanding the impacts of various market scenarios on the viability of competing technology roadmaps instead of predicting specific years in which we anticipate crossover. The uncertainty associated with market forces—minerals pricing, demand growth and geopolitical conflicts—simply makes it too challenging to predict exact timelines with accuracy and is not the key objective. By contrast, our approach enables quantitative evaluation of the relative robustness of certain technology roadmap propositions to withstand potentially disruptive market forces, thereby increasing confidence or challenging assumptions in the risk-reward profile motivating pursuit of technology development. Central to this approach involves deeply engaging with industry practitioners and soliciting feedback reflecting the realities of technology commercialization[46].

Thus, a key outcome from our scenarios modelling is to reveal key trends in the conditions enabling maximum Na-ion techno-economic competitiveness. Figure 5 shows a clustered plot of all 6,048 scenarios categorized by gravimetric energy density and supply chain conditions, where a strong dependence on both factors reasonably describes the modelled timelines to Na-ion Price Advantage over LFP. When supply chain conditions are unfavourable for Li-ion (specifically LFP)—such as high lithium prices, graphite supply shocks or both—Na-ion competitiveness is accelerated across the board. By contrast, when supply chain conditions are unfavourable for Na-ion (specifically nickel-containing chemistries), competitiveness is severely hindered. As indicated by the trends from left to right, pursuing technology development roadmaps that maximize energy densities is important to accelerate timelines to competitiveness. Note that a large subset (2,522) of scenarios do not produce conditions for Na-ion Price Advantage before 2050, represented by the open circles in Fig. 5. Importantly, however, this does not mean that Na-ion is not competitive. A similar clustered plot as Fig. 5 in Supplementary Fig. 63 shows the timelines to Na-ion Price Parity with LFP, illustrating that over 40% of all modelled scenarios reach a Price Parity condition on or before 2030, and the average 'parity period' spans 5.6 ± 3.6 years. With Na-ion being a competitive, viable substitute to Li-ion having similar price curves (assuming that performance parity is achieved), any disruptions to the Li-ion supply chain will likely present Na-ion as an immediately price advantageous alternative.

https://doi.org/10.1038/s41560-024-01701-9

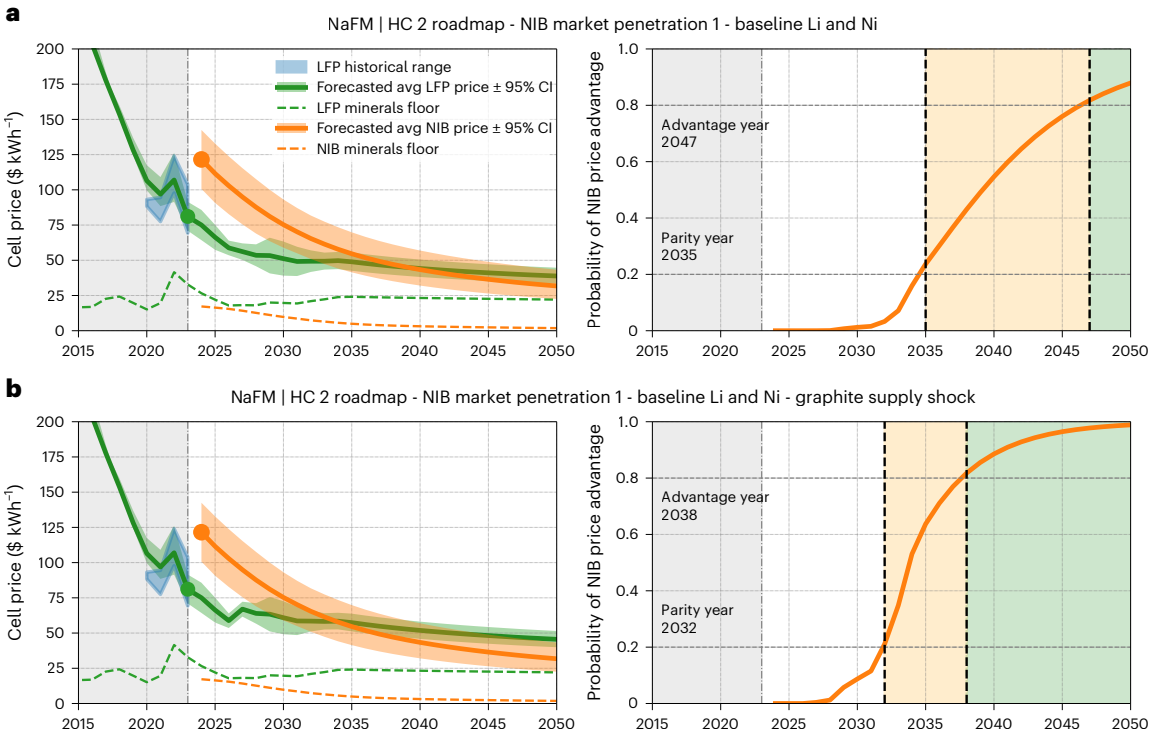

Fig. 4 | Comparative price curve assessments to evaluate techno-economic competitiveness considering hypothetical Li-ion supply chain disruptions. **a**,**b**, Example of Roadmap 'NaFM|HC 2' with a conservative market penetration (NIB Market Penetration 1), baseline lithium and nickel prices, and no graphite supply shock (**a**) or a hypothetical graphite supply shock (**b**) in 2027. Comparative price curves (left) and probability profiles (right) allow evaluation of Price Parity and Price Advantage timelines. The example shown in **b** has a 4-year timeframe (yellow) where Na-ion and LFP are closely competitive, whereas the example in **a** has a 12-year competitive timeframe.

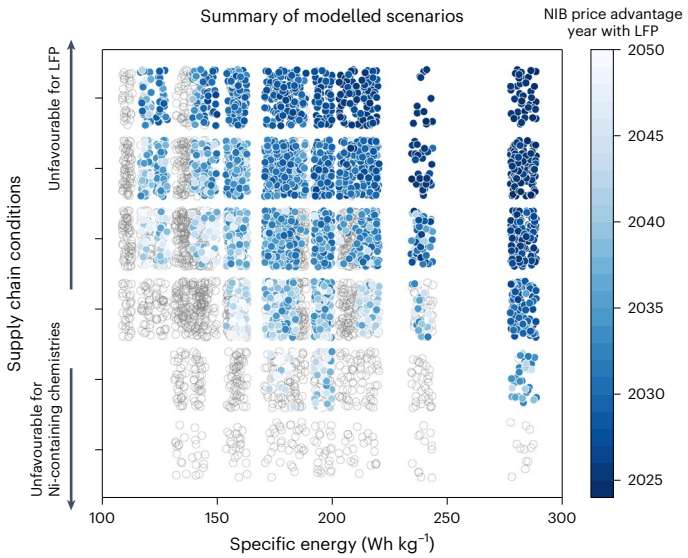

Fig. 5 | Na-ion techno-economic competitiveness highly dependent on supply chain conditions and technology development roadmaps towards higher energy densities. Heatmap showing timelines to Price Advantage. Supply chain conditions ranked categorically here via summation of integer increments/decrements of lithium, graphite and nickel supply chain conditions according to Na-ion favourability—with increased nickel commodity pricing being unfavourable to only nickel-containing Na-ion layered oxide cathodes. For example, a high lithium price scenario (+1) coinciding with a graphite supply shock (+1) will produce a supply chain score of +2. The *x*-axis is ranked by the specific energy density targets achieved by 2030 in the various roadmaps.

For example, if lithium prices increase between now and 2027 and remain high (~$50,000 tonne^{-1} lithium carbonate equivalent (LCE); Supplementary Fig. 8 and Supplementary Note 4), over 55% of all Na-ion technical roadmaps lead to a Price Advantage condition before 2035. By contrast, if lithium minerals prices remain low (around $10,000 tonne^{-1} LCE; Supplementary Fig. 8 and Supplementary Note 4), there will be virtually no Na-ion development scenarios that will result in a Price Advantage condition without a coinciding supply chain disruption in graphite (or potentially other Li-ion specific materials). For reference, the spot price of lithium at the time of this writing (2024) averages $10,000–15,000 tonne^{-1}—the result from oversupply of battery metals owing to a slump in EV sales in the latter half of 2023[7,47]. Whether lithium prices can continue to stay low is thus a question with profound implications, especially on the competitiveness of Na-ion batteries.

The fastest and most certain way for Na-ion to be price advantageous is to reduce materials intensity by increasing materials and cell-level energy densities. This is supported quantitatively in the parameter sensitivity analysis shown in Fig. 6, where some of the biggest drivers of forecasted Na-ion cell prices in 2030 and 2040 are accessible upper voltage cut-offs, cathode and anode specific capacities, and electrode thicknesses. Increasing accessible upper voltage cut-offs (a capability specific to layered oxide cathodes with solid-solution intercalation behaviour) simultaneously increases available specific capacity and the nominal voltage, which unsurprisingly compounds to provide the largest feature importance. However, this is not always an available option owing to material limitations, gas release or challenges with power electronics upon systems integration[25] (see caption in Supplementary Fig. 30). Therefore, increasing specific capacity alone is an important strategy. In nickel-containing cathodes, this can ideally be done in conjunction with minimizing nickel content

https://doi.org/10.1038/s41560-024-01701-9

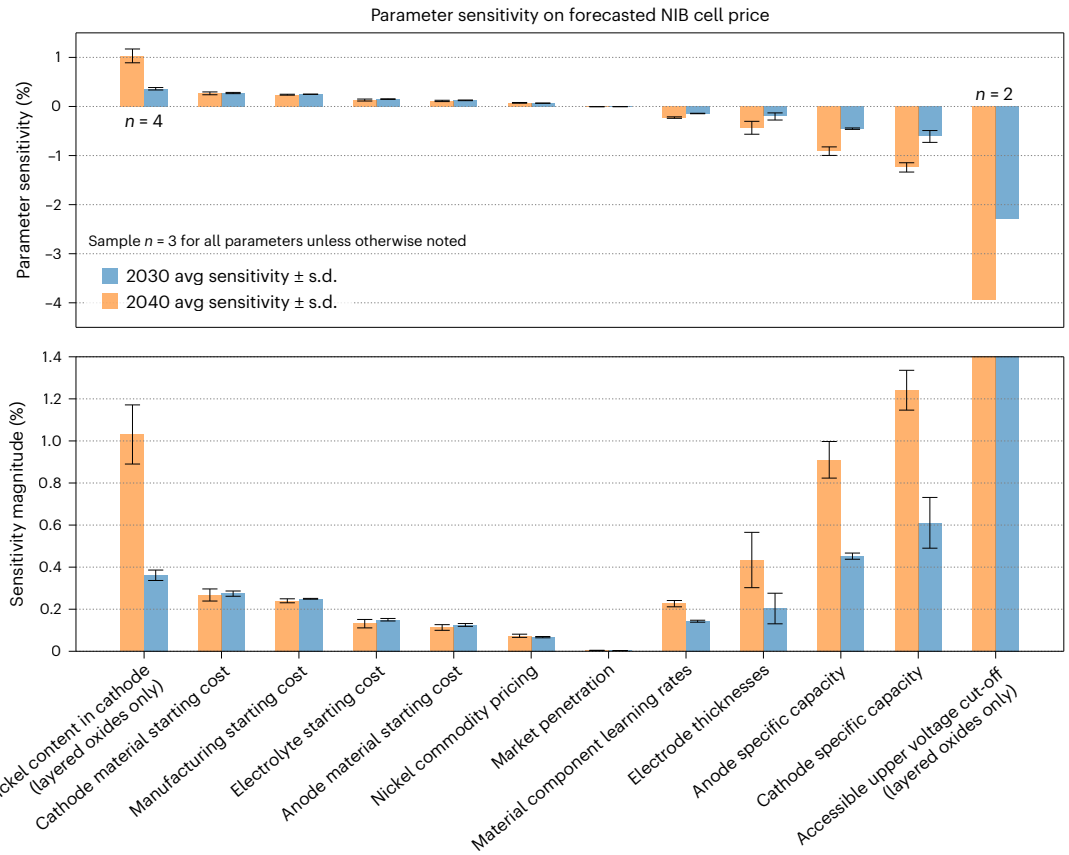

Fig. 6 | Increasing energy densities and reducing critical minerals content are biggest levers to affect Na-ion cell prices. Parameter sensitivity analysis on the relative importance of features affecting Na-ion cell prices in 2030 (blue) and 2040 (orange). Error bars show standard deviation of parameter sensitivity between multiple one-at-a-time (OAT) perturbations, and the bottom plot shows the absolute values of parameter sensitivities to enable comparison. Certain features (for example, reducing nickel content in cathodes and increasing accessible voltage cut-off) are specific to layered oxide cathodes only. A pattern emerges indicating that design directions that increase energy densities (accessible voltage, cathode and anode specific capacities, and electrode thicknesses) are key drivers of price. In addition, the reduction of nickel content in cathodes has a significant impact on the minerals price floor—more so than the absolute price of nickel commodities. These provide guidance on road mapping directions to maximize the techno-economic competitiveness of Na-ion.

owing to its relative feature importance. It is worth noting here that the uncertainties associated with fitted learning rates and starting prices of material components (which are further elaborated in Supplementary Note 3) are unlikely to affect the conclusions significantly owing to the low variability in present-day price assessments compounded with the lower sensitivity of both learning rates and starting costs to the forecasted outcomes as illustrated in Fig. 6.

Increasing the specific capacity of HC anodes is yet another critical design direction identified. With low tap and calender densities, HCs impose practical thickness limitations that relegate a balanced cathode to low areal capacity loadings (mAh cm^{-2}). Knock-on effects include requiring more electrolyte volume to saturate increased porosity within electrodes. In addition, the aggressively slopey voltage profiles of HCs limit the deliverable cell energy, which negatively impacts cost performance[48]. For these reasons, HCs may enable the first generation of Na-ion batteries to demonstrate commercial viability but may require considerable specific capacity improvements (>400 mAh g^{-1}) or outright replacement to enable long-term techno-economic competitiveness with Li-ion.

Replacing HCs with alloying anodes, such as tin, is one approach to substantially increase anode specific capacity. In our models, however, despite a NaNM|Sn baseline cell starting off ~30% lower price than a NaNM|HC cell, its observed price curve appears to fall at a slower rate. This is explained by the minerals price floor and engineering design floor of metallic tin both leaving little room for further improvements on cost and material-level performance. Therefore, alloy-based anodes appear to be effective tools to lower costs in the short term but may require cathode improvements to stay competitive in the long term.

An alternative design direction is to forgo an anode material altogether and opt for an anode-free cell configuration. This of course would require higher-risk innovation but may not require substantial improvements to current-generation Na-ion cathode technology. Roadmap 'NaNM|AF 1', for example, does not assume any improvements to cathode specific capacity and only assumes an increase in areal capacity loadings of state-of-the-art nickel-based layered oxides while maintaining a modest upper cut-off voltage of 4.0 V. However, advanced separators, electrolytes and/or current collectors required to enable anode-free designs must do so without reversing the techno-economic argument. Here we highlight the importance of using such a techno-economic toolkit to drive research decision-making as opposed to applying it post facto.

Finally, despite NFPP cathodes being less than half the cost of NNM and exhibiting a low minerals floor, the confluence of three technical parameters—low specific capacity, low tap density and low voltage—presents challenges to outright advantage on a \$ kWh^{-1} basis. Its volumetric capacity (mAh cm^{-3}) is even lower than that of HCs, which results in low areal capacity loadings. Necessary routes to compete therefore likely require dry electrode processing to enable ultra-thick electrodes and incorporating alloy-based anodes to increase energy density. However, we again note that cell-level prices do not adequately capture other critical performance features, and NFPP-based Na-ion cells may

prove more competitive at the systems level if safety, thermal robustness and cycle life metrics can be demonstrated to exceed those of LFP.

Both Figs. 5 and 6 illustrate that technical development roadmaps are not only beneficial but also imperative to Na-ion's techno-economic competitiveness. Relying solely on learning-by-doing from scaling the production of material components is insufficient to compete with the rapidly evolving Li-ion trends. Therefore, adjusting between the most conservative and aggressive market penetration scenarios yielded minimal feature importance on future Na-ion prices. Similarly, adjusting material component learning rates to higher-than-typical ('Aggressive') values of 20 ± 3% for the Na-ion cathode, anode and electrolyte also had modest feature importance. These observations suggest that engineering advancements are a greater lever to affect prices than the limited room for materials price reductions via learning-by-doing. This increases the likelihood of competitiveness, as price reductions do not rely on a chicken-and-egg problem with capturing market share.

In closing, Na-ion deserves considerable research, development and commercialization attention. We caution against assumptions and promises of immediate or near-term (pre-2030) price advantage against Li-ion, specifically LFP, but believe that it has a critical role to play in the energy transition as a viably scalable Li-ion substitute under circumstances of supply chain volatility. Therefore, we believe investing in Na-ion development roadmaps to maintain a competitive track with Li-ion would be prudent. In the same vein, investments in Li-ion supply chain security should not be foregone given the demonstrated sensitivity to supply shocks.

The ultimate objective of developing low-cost batteries is to enable rapid deployment of energy storage in vehicular and stationary applications to meet the needs of the energy transition. These goals must be met even in the face of rising geopolitical tensions and supply chain volatilities. It is therefore not only important to accurately forecast price trends for incumbent technologies but also critical to understand competitive or substitutional opportunities for emerging technologies. Our proposed modelling framework herein enables such an approach. Modelled outcomes help guide research endeavours and inform strategic investments commensurate with the probability of techno-economic competitiveness and commercial success.

Methods

Componential floor-constrained learning curves

The typical Wright's learning curve follows the form

$$Y = Ax^{-b} \tag{1}$$

where the price of a technology Y at a given cumulative experience x is described by the price of the first unit A and a rate of price reduction b. Here the learning rate (or experience rate) is defined as the percentage price reduction after every doubling of cumulative experience, given by

$$\mathrm{LR} = 1 - 2^{-b} \tag{2}$$

As established above, these curves have been demonstrated to accurately capture the price trends across various sectors in a technology-agnostic manner, but they can also overestimate price reductions when technologies approach their price floors dictated by physical limits. In such scenarios, the equation can be modified to incorporate a floor constraint, shown by

$$Y = (A_0 - A_{\mathrm{floor},0})\left(\frac{x_t}{x_0}\right)^{-b} + A_{\mathrm{floor,t}} \tag{3}$$

Here $A_{\mathrm{floor},0}$ and $A_{\mathrm{floor,t}}$ illustrate that the price floors can evolve dynamically with time. Cumulative experience is also normalized for a more practical implementation of the general form in equation (1) that enables one to use the known price and cumulative 'incurred' experience of components in the present and backcast and forecast accordingly. It also enables us to use actual quantities produced (in kT or Mm^2, for example) in fitting historical data where such production data is available, and switch to using anticipated demand (in GWh) in projecting future price trends. Agreement on present pricing is therefore all that is required to yield continuity between historical and forecasted prices. In this paper, we implement dynamically varying minerals price floors obtained from historical and forecasted price trends to capture the price evolution of individual component costs of a battery. This enables us to capture individual learning rates, market growth rates and price floors between material components, which are unlikely to always be the same.

Physically accurate technology roadmaps

To capture the evolution of materials intensities within cell designs owing to technical advancements in materials performance and cell engineering, we implement a modified Moore's law to capture improvements as a function of time. We first model physically accurate cell designs via bottoms-up modelling to obtain exact materials intensities for each component (in kg kWh^{-1} or m^2 kWh^{-1}) based on the bill-of-materials. Cell designs are then assigned to specific years that represent the requisite technological progress, and we fit a curve with an asymptotic limit defined by theoretical or practical engineering limits. The curve follows the form

$$M = M_{\mathrm{min}} + \mathrm{A}e^{-b*(t-t_0)} \tag{4}$$

where M_{min} is defined by equations (6)–(11) for each material component. Here the cathode and anode minimum materials intensities are defined by their respective maximum theoretical specific capacities and allowable electrode thicknesses. The minimum electrolyte materials intensity is defined by the total pore volume within the electrodes only. The minimum separator materials intensity (in m^2 kWh^{-1}) is defined by a maximum cathode thickness and therefore capacity loading. The minimum positive and negative current collector materials intensities are then calculated from the separator materials intensity but converted to a mass basis (kg kWh^{-1}) based on the densities and minimum practical thicknesses of the foils. For the other material components category, the asymptotic limit M_{min} is omitted as there is no basis for a minimum limit. In a similar fashion, the maximum theoretical cell-level specific energy is calculated by summing up a balanced anode- or cathode-limited unit-cell based on the provided limits, where equation (4) is modified to approach an asymptotic maximum as opposed to a minimum, with the form

$$\mathrm{SE} = \mathrm{SE}_{\mathrm{max}} - Ae^{-b*(t-t_0)} \tag{5}$$

The equations defining the calculation of minimum materials intensities is as follows:

$$M_{\mathrm{CAT_{theo}}}\left[\frac{\mathrm{kg}}{\mathrm{kWh}}\right] = \frac{1}{q_{\mathrm{CAT_{theo}}}}\left[\frac{\mathrm{g}}{\mathrm{mAh}}\right] \times \frac{1}{E_{\mathrm{cell}}}\left[\frac{1}{\mathrm{V}}\right] \tag{6}$$

$$M_{\mathrm{AND_{theo}}}\left[\frac{\mathrm{kg}}{\mathrm{kWh}}\right] = \frac{1}{q_{\mathrm{AND_{theo}}}}\left[\frac{\mathrm{g}}{\mathrm{mAh}}\right] \times \frac{1}{E_{\mathrm{cell}}}\left[\frac{1}{\mathrm{V}}\right] \tag{7}$$

$$M_{\mathrm{ELY_{theo}}}\left[\frac{\mathrm{kg}}{\mathrm{kWh}}\right] = \rho_{\mathrm{ELY}}\left[\frac{\mathrm{g}}{\mathrm{cm^3}}\right] \times \left\{\frac{\varepsilon_{\mathrm{CAT_{min}}}[\%]}{\rho_{\mathrm{CAT_{theo}}}[\mathrm{g/cm^3}] \times q_{\mathrm{CAT_{theo}}}[\mathrm{mAh/g}]} + \mathrm{NP_{Ratio}} \times \frac{\varepsilon_{\mathrm{AND_{min}}}[\%]}{\rho_{\mathrm{AND_{theo}}}[\mathrm{g/cm^3}] \times q_{\mathrm{AND_{theo}}}[\mathrm{mAh/g}]}\right\} \times \frac{1}{E_{\mathrm{cell}}}\left[\frac{1}{\mathrm{V}}\right] \tag{8}$$

$$M_{\mathrm{SEP_{theo}}}\left[\frac{\mathrm{m^2}}{\mathrm{kWh}}\right] = \frac{2}{t_{\mathrm{CAT_{max}}}[\mathrm{m}] \times \rho_{\mathrm{CAT_{theo}}}[\mathrm{g/cm^3}] \times q_{\mathrm{CAT_{theo}}}[\mathrm{mAh/g}] \times (1 - \varepsilon_{\mathrm{CAT_{min}}}[\%])} \times \frac{1}{E_{\mathrm{cell}}}\left[\frac{1}{\mathrm{V}}\right] \tag{9}$$

$$M_{\mathrm{PCC}_{\mathrm{theo}}}\left[\frac{\mathrm{kg}}{\mathrm{kWh}}\right]=M_{\mathrm{SEP}_{\mathrm{theo}}}\left[\frac{\mathrm{m}^2}{\mathrm{kWh}}\right]\times\rho_{\mathrm{PCC}_{\mathrm{theo}}}\left[\mathrm{g/cm}^3\right]\times t_{\mathrm{PCC}_{\mathrm{min}}}\left[\mu\mathrm{m}\right] \quad (10)$$

$$M_{\mathrm{NCC}_{\mathrm{theo}}}\left[\frac{\mathrm{kg}}{\mathrm{kWh}}\right]=M_{\mathrm{SEP}_{\mathrm{theo}}}\left[\frac{\mathrm{m}^2}{\mathrm{kWh}}\right]\times\rho_{\mathrm{NCC}_{\mathrm{theo}}}\left[\mathrm{g/cm}^3\right]\times t_{\mathrm{NCC}_{\mathrm{min}}}\left[\mu\mathrm{m}\right] \quad (11)$$

For each material component, the A and b parameters in equation (4) are fitted after the M_{min} parameter is calculated. Occasionally, when one parameter is assumed to not experience marked improvements, such as the specific capacity of graphite (current values ~360 mAh g^{-1} are already near the theoretical capacity), the fitted parameter b may end up <0, making the exponential term >0 with a very shallow slope. This is an artefact of fitting, and we do not expect actual material performance to decline with time. Therefore, in cases where the fitted b parameter ends up negative, we instead use a flat line with zero slope centred at the average of the fitted values. The engineering limits used in our modelling are summarized in Supplementary Table 4.

Combining the modified Wright's law with the modified Moore's law

After having established (a) floor-constrained learning curves and (b) materials intensities for each component scaling as a function of cumulative experience and time, respectively, we can combine them to produce a generalized equation, which captures the overall cell price. This is represented in general form as

$$Y_{\mathrm{cell}}=\left(\sum_{n}^{k}M_{n,t}\times\left[(a_{n_0}-a_{n_{\mathrm{floor},0}})\left(\frac{x_{n,t}}{x_{n,0}}\right)^{-b_n}+a_{n_{\mathrm{floor},t}}\right]\right)+a_{\mathrm{mfg}}\left(\frac{x_{\mathrm{mfg},t}}{x_{\mathrm{mfg},0}}\right)^{-b_{\mathrm{mfg}}} \quad (12)$$

The first term of the right-hand side aggregates the individual material component costs of a battery cell, each defined by its own learning rate, $-b_n$, normalized cumulative experience, $\left(\frac{x_{n,t}}{x_{n,0}}\right)$, price floor, $a_{n_{\mathrm{floor},t}}$, and a material intensity scalar, $M_{n,t}$, that captures the kg kWh^{-1} or m^2 kWh^{-1} contribution required for the representative modelled cell design. Here $n\in$ positive active material, negative active material, electrolyte, separator, positive current collector, negative current collector and others. While in practice, all material components will have hard physical limits of a price floor, some components have negligible minerals costs, including polyolefins and conductive carbons. Therefore, for those materials, $a_{n_{\mathrm{floor},t}}$ and $a_{n_{\mathrm{floor},0}}$ are zeroed. The second term of the right-hand side captures the costs associated with manufacturing, including equipment depreciation, labour, scrap, SG&A, other overheads, warranty and profit. Notably, this second term is an unconstrained learning curve as there is no direct physical basis to institute a hard price floor. One may consider implementing manufacturing CapEx as a potential price floor, but as we do not yet have a clear methodology to firmly establish a minimum, we leave it unconstrained in this paper. Note that the learning parameter associated with manufacturing costs inherently captures other technical factors such as processing yield improvements and economies-of-scale, which we do not further resolve in our current work. See Supplementary Fig. 64 for fitting details. The materials intensity scalar is used to capture the improvements to cell design and active materials specific capacities, both of which are key contributors to historic cell price declines. This componential approach captures the nuance that different components of a battery will experience different materials improvements, learn at different rates, experience different market growth scenarios and be constrained by respectively different floors.

The above learning curves can be correlated with time by defining individual component market growth rates. Here we use Gompertz sigmoidal functions to describe the annual demand of individual battery components, as they provide better fits to market projections than standard logistic functions[18]. The annual production capacity at year t can be defined as

$$q_{n,t}=q_{n,\mathrm{base}}\exp\left[\ln\left(\frac{q_{n,\mathrm{sat}}}{q_{n,\mathrm{base}}}\right)(1-\exp\left[-r_n t\right])\right] \quad (13)$$

where $q_{n,\mathrm{base}}$, $q_{n,\mathrm{sat}}$ and r_n represent the starting annual production capacity, the annual production capacity upon market saturation and growth rate of component n, respectively. Notably, not all battery components experience the same market growth conditions. For example, whereas the demand for graphite materials in tonnes per annum scales closely with the cumulative demand of total Li-ion batteries owing to it being the predominant anode chemistry, LFP and NMC materials will each scale at a lower rate owing to their fractional market share. With this, the cumulative capacity can be obtained from

$$x_{n,t}=\sum_{t=0}^{T}q_{n,t} \quad (14)$$

Minerals pricing

Each mineral dataset was converted into aggregate averages with a sample size of $n\geq 3$ if including proprietary industry sources, or $n=1$ if data was only available from USGS. Owing to the proprietary nature of each of the industry-supplied forecasts, the minerals pricing datasets are averaged at each time step with 95% CI to prevent traceability to any one data source using the formula

$$\mu\pm 1.96\frac{\sigma}{\sqrt{n}} \quad (15)$$

While USGS datasets do not provide minerals price forecasts, industry intelligence firms do, and we use their 2023 forecasts as our baseline scenario for the key minerals (lithium, nickel, cobalt and so on) looking forward. As expected, there is good agreement on historical minerals pricing but notably larger variances between forecasts within the next decade. Owing to inherently large uncertainties associated with forecasting prices of volatile minerals, we also perform analysis of self-generated fixed price scenarios (for example, high/mid/low) on the key commodities to evaluate the sensitivity of outcomes (Supplementary Note 4 and Supplementary Figs. 8 and 9).

Historical material component pricing

All prices obtained from industry and literature were inflation-adjusted to USD2023. For any year with multiple data points, averages and CIs were calculated using the same methodology above. For tabulating annual production quantities (in kT or Mm^2), gaps in data were interpolated using the requisite compound annual growth rates (CAGRs) established by the bounding years for which data was available, where CAGR is defined by

$$\mathrm{CAGR}=\left(\frac{P_2}{P_1}\right)^{1/t}-1 \quad (16)$$

Cell modelling

To accurately model cells, representative half-cell voltage versus specific capacity (mAh g^{-1}) curves of positive and anode material candidates (for example, LFP, NMC622, NMC811 and graphite) were extracted from literature and were mathematically scaled to meet target electrode coating mass loadings, active mass fractions, areal capacity loadings and calender densities (and therefore porosities). Importantly, first cycle (de)lithiation or (de)sodiation curves were utilized in order to capture differences in first cycle efficiencies between positive and negative electrode pairings, and full cell voltage curves were obtained by subtracting negative from positive. This approach

is critical to obtaining accurate predictions of realizable energy densities[48] (Supplementary Fig. 65). Cell modelling details are discussed at length in Supplementary Note 9, along with validation against experimental data in Supplementary Note 10, Supplementary Table 5 and Supplementary Figs. 66 and 67.

Once the electrode balancing procedure is completed to obtain accurate unit cell designs, the electrode parameters were inputted to the BatPaC (v5.1) spreadsheet model produced by Argonne National Laboratory[22] to obtain exact mass and areal quantities per stored energy content (kg kWh^{-1} or m^2 kWh^{-1}). In addition, we leverage the detailed manufacturing cost calculations within BatPaC to obtain the present-day manufacturing costs on a per-kWh basis. We take this approach for the following reasons. (1) Despite being highly detailed in modelling manufacturing-related costs, BatPaC has shortcomings in capturing the true voltage, capacity and energy characteristics of cells owing to inherent limitations of a spreadsheet approach. Especially considering occasional mismatched first cycle efficiencies between cathode and anode pairings and uniquely slopey or stepped voltage curves of emerging Na-ion materials, the true energy (Wh)—which is the area underneath the voltage curve between capacity and voltage windows—can often be miscalculated. This may result in errors in calculating true \$ kWh^{-1} (ref. 48). (2) We note that BatPaC only models large format (>60 Ah) pouch cells, whereas some of the cells modelled (for example, Tesla 4680 cylindrical cells) do not share the same format. However, we replicate all cell designs using BatPaC to enable systematic comparisons across generations and chemistries, and we also note that materials intensity, energy densities and manufacturing costs at the GWh scale will not deviate substantially between formats. This general approach allows us to systematically evaluate new cell designs and obtain cell manufacturing costs associated with each design while being more nuanced in electrode balancing. See Supplementary Note 11 for details on BatPaC Modifications made in our modelling efforts.

Current Na-ion material price assessment survey

To obtain present-day pricing of materials used in the nascent industry of Na-ion batteries, we take the approach of surveying industry experts and reports with insights on actual current-day pricing[24,25]. We survey from $n = 11$ sources on the key material components used in Na-ion batteries. Not all sources were able to provide estimates for every material component, but most material components had at least $n = 3$ sources. If a given source provided a range of pricing corresponding to a low and high estimate, both values were used to appropriately weight the samples instead of the mid-range value. Specifically for biomass- and phenolic resin-based HC materials, which can currently be sourced from producers in China and Japan at substantially disparate costs, we also delineate which region the prices are quoting. In our modelling, we only use prices from China given the substantially higher concentration of Na-ion commercialization activity in that region. The results of our pricing survey are shown in Fig. 3b.

Data availability

The minerals prices and forecasts, cell price assessments, material price assessments and market size forecasts are provided from third-party industry sources that have contributed to this work and are individually considered proprietary. However, aggregate averages and confidence intervals are published in this work, and such data are available in Excel format in the Supplementary Information. Source data are provided with this paper.

References

1. *Electric Vehicle & Battery Supply Chain: Strategic Planning Outlook to 2050* (Wood Mackenzie, 2023).
2. Pillot, C. *The Rechargeable Battery Market and Main Trends 2022–2030* (Avicenne Energy, 2023).
3. *Lithium-Ion Battery Pack Prices Rise for First Time to an Average of $151/kWh* (BloombergNEF, 2022); https://about.bnef.com/blog/lithium-ion-battery-pack-prices-rise-for-first-time-to-an-average-of-151-kwh/
4. Ziegler, M. S. & Trancik, J. E. Re-examining rates of lithium-ion battery technology improvement and cost decline. *Energy Environ. Sci.* **14**, 1635–1651 (2021).
5. Ziegler, M. S., Song, J. & Trancik, J. E. Determinants of lithium-ion battery technology cost decline. *Energy Environ. Sci.* **14**, 6074–6098 (2021).
6. *Benchmark Cell Prices Assessment* (Benchmark Mineral Intelligence, 2024).
7. Khan, Y. Low battery metal prices set to persist in 2024, adding friction to energy transition. *The Wall Street Journal* https://www.wsj.com/articles/low-battery-metal-prices-set-to-persist-in-2024-adding-friction-to-energy-transition-3773ba00 (2023).
8. Stoikou, E. Battery prices are falling again as raw material costs drop. *Bloomberg* https://www.bloomberg.com/news/articles/2023-11-26/battery-prices-are-falling-again-as-raw-material-costs-drop (27 November 2023).
9. Lee, A. Nickel price crash seen extending Indonesia's grip on supply. *Bloomberg* https://www.bloomberg.com/news/articles/2024-01-22/nickel-price-crash-seen-strengthening-indonesia-s-grip-on-supply (22 January 2024).
10. McNulty, R. & Williams, E. OPINION: why sodium ion batteries will take longer than people think. *Benchmark Source* https://source.benchmarkminerals.com/article/opinion-why-sodium-ion-batteries-will-take-longer-than-people-think (2023).
11. Wright, T. P. Factors affecting the cost of airplanes. *J. Aeronaut. Sci.* **3**, 122–128 (1936).
12. Nagy, B., Farmer, J. D., Bui, Q. M. & Trancik, J. E. Statistical basis for predicting technological progress. *PLoS ONE* **8**, e52669 (2013).
13. Schmidt, O., Melchior, S., Hawkes, A. & Staffell, I. Projecting the future levelized cost of electricity storage technologies. *Joule* **3**, 81–100 (2019).
14. Schmidt, O., Hawkes, A., Gambhir, A. & Staffell, I. The future cost of electrical energy storage based on experience rates. *Nat. Energy* **2**, 17110 (2017).
15. Frith, J. T., Lacey, M. J. & Ulissi, U. A non-academic perspective on the future of lithium-based batteries. *Nat. Commun.* **14**, 420 (2023).
16. Nykvist, B. & Nilsson, M. Rapidly falling costs of battery packs for electric vehicles. *Nat. Clim. Change* **5**, 329–332 (2015).
17. Kittner, N., Lill, F. & Kammen, D. M. Energy storage deployment and innovation for the clean energy transition. *Nat. Energy* **2**, 17125 (2017).
18. Hsieh, I.-Y. L., Pan, M. S., Chiang, Y.-M. & Green, W. H. Learning only buys you so much: practical limits on battery price reduction. *Appl. Energy* **239**, 218–224 (2019).
19. McNerney, J., Doyne Farmer, J. & Trancik, J. E. Historical costs of coal-fired electricity and implications for the future. *Energy Policy* **39**, 3042–3054 (2011).
20. Way, R., Ives, M. C., Mealy, P. & Farmer, J. D. Empirically grounded technology forecasts and the energy transition. *Joule* **6**, 2057–2082 (2022).
21. Nemet, G. F. Beyond the learning curve: factors influencing cost reductions in photovoltaics. *Energy Policy* **34**, 3218–3232 (2006).
22. Knehr, K. W., Kubal, J. J., Nelson, P. A. & Ahmed, S. *Battery Performance and Cost (BatPaC) v5.1 Spreadsheet Model* (Chemical Sciences and Engineering Division, Argonne National Lab, 2022).
23. Wang, A. & Yiu, N. *Battery Component Price Report December 2023* (Intercalation Station, 2023).
24. Jephcott, B. *Sodium-Ion Battery Market Research Report* (Golden Dragon Capital, 2024).

25. Barker, J. et al. *Industry Expert Panel* (Personal Communication, 2024).
26. *Anode Prices* (Benchmark Mineral Intelligence, 2024).
27. *Cathode Prices* (Benchmark Mineral Intelligence, 2024).
28. *Minerals Price Forecasts* (Benchmark Mineral Intelligence, 2024).
29. *Battery Materials Pricing Data* (S&P Capital IQ, 2023).
30. *Mineral Commodity Summaries 2024* (United States Geological Survey, 2024); https://www.usgs.gov/centers/national-minerals-information-center/mineral-commodity-summaries
31. Stock, S. et al. Cell teardown and characterization of an automotive prismatic LFP battery. *Electrochim. Acta* **471**, 143341 (2023).
32. Ank, M. et al. Lithium-ion cells in automotive applications: Tesla 4680 cylindrical cell teardown and characterization. *J. Electrochem. Soc.* **170**, 120536 (2023).
33. Günter, F. J. & Wassiliadis, N. State of the art of lithium-ion pouch cells in automotive applications: cell teardown and characterization. *J. Electrochem. Soc.* **169**, 030515 (2022).
34. Barnett, B. et al. *PHEV Battery Cost Assessment* (TIAX LLC, 2010).
35. Gallagher, K. G. & Nelson, P. A. in *Lithium-Ion Batteries* (ed. Pistoia, G.) 97–126 (Elsevier, 2014).
36. Lain, M. J., Brandon, J. & Kendrick, E. Design strategies for high power vs. high energy lithium ion cells. *Batteries* **5**, 64 (2019).
37. Tarascon, J.-M. Na-ion versus Li-ion batteries: complementarity rather than competitiveness. *Joule* **4**, 1616–1620 (2020).
38. Xu, Z.-L. et al. Tailoring sodium intercalation in graphite for high energy and power sodium ion batteries. *Nat. Commun.* **10**, 2598 (2019).
39. Zhang, B. et al. Microsized Sn as advanced anodes in glyme-based electrolyte for Na-ion batteries. *Adv. Mater.* **28**, 9824–9830 (2016).
40. Yang, T., Luo, D., Liu, Y., Yu, A. & Chen, Z. Anode-free sodium metal batteries as rising stars for lithium-ion alternatives. *iScience* **26**, 105982 (2023).
41. Chen, Y. et al. Prospects for practical anode-free sodium batteries. *Mater. Today* https://doi.org/10.1016/j.mattod.2024.01.002 (2024).
42. Rudola, A. et al. Commercialisation of high energy density sodium-ion batteries: Faradion's journey and outlook. *J. Mater. Chem. A* **9**, 8279–8302 (2021).
43. Barker, J. *The Path to the Successful Commercialization of Sodium-Ion Batteries*. *Stanford StorageX International Symposium* (Stanford University, 2022).
44. Rudola, A., Sayers, R., Wright, C. J. & Barker, J. Opportunities for moderate-range electric vehicles using sustainable sodium-ion batteries. *Nat. Energy* **8**, 215–218 (2023).
45. Farmer, J. D. & Lafond, F. How predictable is technological progress? *Res. Policy* **45**, 647–665 (2016).
46. Yao, A., Benson, S. M. & Chueh, W. C. How quickly can sodium-ion learn? Assessing scenarios for techno-economic competitiveness against lithium-ion batteries. Preprint at https://arxiv.org/abs/2403.13759 (2024).
47. Liu, S. & Patton, D. China lithium price poised for further decline in 2024—analysts. *Reuters* https://www.reuters.com/markets/commodities/china-lithium-price-poised-further-decline-2024-analysts-2023-12-01/ (2023).
48. Innocenti, A., Beringer, S. & Passerini, S. Cost and performance analysis as a valuable tool for battery material research. *Nat. Rev. Mater*. https://doi.org/10.1038/s41578-024-00657-2 (2024).

Acknowledgements

This work was supported by three offices within the US Department of Energy through the STEER Program, a partnership between the SLAC-Stanford Battery Center and the Stanford Precourt Institute for Energy. Specifically, the three offices are the Office of Electricity, the Vehicle Technologies Office under the Office of Energy Efficiency and Renewable Energy, and the Office of Technology Transitions. In addition, this work was supported in part by the National Science Foundation Graduate Research Fellowship Program (award number DGE-2146755; A.Y.). We thank the panel of industry consultants/experts cited throughout the work, including those that provided written feedback/critique of the paper draft[46]. They include J. Barker, C. Wessells (Natron Energy), B. Kelly (Peak Energy), S. Gore (Bedrock Materials), A. Wang, D. Tan (Unigrid), L. Jing (Tesla), T. Evans (Mana Battery), N. Singstock (Mana Battery), H. A. S. Platt (Mana Battery), K. He (TDK Ventures), F. Renard (Avicenne Energy), C. Pillot (Avicenne Energy), W. Yen (LongTime Technologies), W. Hwang (LongTime Technologies), K. Rodby (Volta Energy Technologies), S. Lux (Universität Münster), J. Wesselkämper (Universität Münster), P. Voß (Universität Münster), C. Parker (Ratel Consulting), M. Munjal (MIT), the Boston Consulting Group and B. Spatocco (Lucid Motors). We finally thank K. Bhuwalka, H. Ramachandran, J. Frohmann and A. Geslin for their thoughtful comments and feedback on the paper. We especially thank K. Bhuwalka and H. Ramachandran for collecting formal responses and summarizing learnings from industry convenings[46].

Author contributions

A.Y.: conceptualization, methodology, modelling, data gathering, data contributor relations, data curation, analysis, visualization, writing, project administration and funding acquisition. S.M.B.: conceptualization, resources, review, editing, supervision and funding acquisition. W.C.C.: conceptualization, resources, review, editing, supervision and funding acquisition.

Competing interests

A.Y. is among the founders of EnPower, a manufacturer of Li-ion batteries. W.C.C. is among the founders of Mitra Chem, a developer of LFP cathode materials. The other authors declare no competing interests.

Additional information

Supplementary information The online version contains supplementary material available at https://doi.org/10.1038/s41560-024-01701-9.

Correspondence and requests for materials should be addressed to Adrian Yao or William C. Chueh.

Peer review information *Nature Energy* thanks the anonymous reviewers for their contribution to the peer review of this work.